Eur. Phys. J. B **42**, 483–490 (2004)
DOI: 10.1140/epjb/e2005-00006-x

THE EUROPEAN PHYSICAL JOURNAL B

# Epitaxial growth of solution deposited $YBa_2Cu_3O_{7-\delta}$ films

O.F. Göbel[1], X. Du[1,a], T. Hibma[1], I. von Lampe[2], F. Zygalsky[2], and U. Steiner[1,3,b]

[1] Materials Science Center, University of Groningen, Nijenborgh 4, 9747 AG Groningen, The Netherlands
[2] Institut für Werkstoffwissenschaften und -technologien, Technische Universität Berlin, Englische Strasse 20, 10587 Berlin, Germany
[3] Department of Physics, University of Cambridge, Madingley Road, CB3 0HE Cambridge, UK

Received 8 June 2004
Published online 18 January 2005 – 

**Abstract.** The solution deposition of $YBa_2Cu_3O_{7-\delta}$ (Y123) high temperature superconducting thin films was studied. The films were prepared from a polymer-containing precursor onto $SrTiO_3$ (001) and $LaAlO_3$ (001) substrates and mineralized at high temperatures. The process depended on details of the film preparation in a delicate fashion, resulting either in superconducting or non-superconducting thin films. To elucidate this difference in conductivity, scanning electron microscopy and several X-ray diffraction techniques were used to characterize the resulting Y123 layers. Both the morphology of the film and the percentage of non-superconducting minority components are likely to be the origin of the difference in the conductance behavior at low temperatures.

**PACS.** 81.15.-z Methods of deposition of films and coatings; film growth and epitaxy – 74.72.-h Cuprate superconductors (high-$T_c$ and insulating parent compounds)

## 1 Introduction

High-temperature superconducting materials have rapidly progressed since their discovery in 1986, and several technological applications have emerged. $YBa_2Cu_3O_{7-\delta}$ (Y123) has been identified as one of the compounds with the highest commercial potential, mainly due to its high critical current density [1]. The commercial success of high-$T_c$ superconducting materials depends on the ability to manufacture films with a thickness considerably above $1\,\mu$m and current densities above $10^5\,A/cm^2$ [1]. This requires the detailed control of the Y123 film deposition techniques. Commonly used methods include laser ablation [2,3], electron-beam evaporation [4], chemical vapor deposition [5,6], or magnetron sputtering [7]. While these well established methods produce Y123 films of a very high quality, they are typically slow, expensive, and not easily combinable with soft lithographic techniques.

Less well known are chemical non-vacuum techniques. These include chemical solution deposition processes, which employ a precursor solution of the constituent metal ions that is solidified during the film manufacture process. It was demonstrated that epitaxial thin films of Y123 can be grown from organic precursor solutions of alkoxides, isopropanol and acetic acid [8], of acetates, 1,3-bis(dimethylamino)-2-propanol and acetic acid [9], of acetates and acetic acid [10], or poly(acrylic acid) (PAA) or poly(methacrylic acid) (PMAA) [11].

Polymer containing precursor solutions are particularly useful, since their viscosity can be adjusted by varying the molecular weight of the polymers, leaving the chemical composition unchanged. Highly viscous solutions can be used in various processes to replicate lateral patterns into the film. These include various soft-lithographic techniques, such as micro-molding [12], and pattern replication using electric fields [13] or temperature gradients [14].

The successful application of chemical solution deposition processes to manufacture high-$T_c$ superconducting thin films requires the control of the morphology and epitaxial alignment of the superconducting phase on the substrate. To this end, we have investigated in detail the epitaxy of Y123 films made by a solution deposition process. Scanning electron microscopy was used to study the film morphology and various X-ray diffraction techniques were employed to investigate the epitaxial order of the Y123 films.

## 2 Experimental details

### 2.1 Sample preparation

Y123 precursor solutions were made following the procedure by von Lampe and coworkers [15]. All

[a] *Present address:* University of Electronic Science and Technology of China, School of Microelectronics and Solid-State Electronics, Chengdu, Sichuan 610051, P.R. China
[b] e-mail: us222@phy.cam.ac.uk

chemicals were purchased from Aldrich or Fluka, with a purity of 98% or higher. $Y(NO_3)_3 \cdot 4H_2O$, $Ba(NO_3)_2$, and $Cu(NO_3)_2 \cdot 2.5H_2O$ were dissolved in N,N-dimethylformamide in a ratio of 1:1.51:2.01 by weight, corresponding to a molar ratio of 1:2:3. Two batches of solution were made according to the same protocol.

The solutions were stirred until clear and poly(methacrylic acid) (PMAA, synthesized according to a protocol in [16]) was added. For Batch 1, the PMAA molecular weight was $M_w \approx 150\,kg/mol$, for Batch 2, $M_w \approx 80\,kg/mol$. This resulted in clear, blue-green solutions with a weight composition (metal-nitrates+PMAA:solvent) of 0.25:1 (Batch 1) and 0.46:1 (Batch 2).

The substrates were polished $SrTiO_3$- and $LaAlO_3$-(001) single crystals[1] ($10 \times 10 \times 1\,mm^3$, with edges parallel to [100], [010], and [001], TBL-Kelpin, Neuhausen, Germany, and Crystec GmbH, Berlin, Germany). Before use, the substrate surfaces were cleaned by heating to 950 °C for several hours in air.

Y123 precursor solutions were spin-cast onto the substrates at 3000 rpm and dried for 2−3 h at 80 °C (Batch 1) and for 1 h at 180 °C (Batch 2). The dried films had a blue-green color. They were placed in a tube-oven, through which a nitrogen-flow was maintained and the temperature was varied according to the following protocol. Batch 1: increase from room temperature to 200 °C with 10 °C/min, from 200 °C to 500 °C with 5 °C/min, from 500 °C to 950 °C with 10 °C/min. The sample was kept at 950 °C for 1 h, and then cooled from 950 °C to ≈600 °C with 5 °C/min, followed by slow cooling to room temperature. When the temperature reached ≈800 °C during heating the gas flow was changed from nitrogen to oxygen. The heating protocol used for the samples of Batch 2 was similar. Argon was used instead of nitrogen and the maximum temperature was ≈750 °C. The gas flow was changed from argon to oxygen upon reaching the maximum temperature.

The obtained films had a thickness of 90−100 nm and were bright gray and transparent.

## 2.2 Scanning electron microscopy

The surface morphology of the annealed films was imaged with a Jeol 6320F field emission scanning electron microscope, using an acceleration voltage of 1.5 kV and a working distance of 5−7 mm.

Figure 1 shows a comparison of a film of Batch 1 (a) and Batch 2 (b). The morphology of the two films was quite different, despite the similarly prepared precursors solutions and the similar sample preparation procedures. The film in Figure 1a is highly porous. It consists of a laterally percolating assembly of crystallites. All crystallites

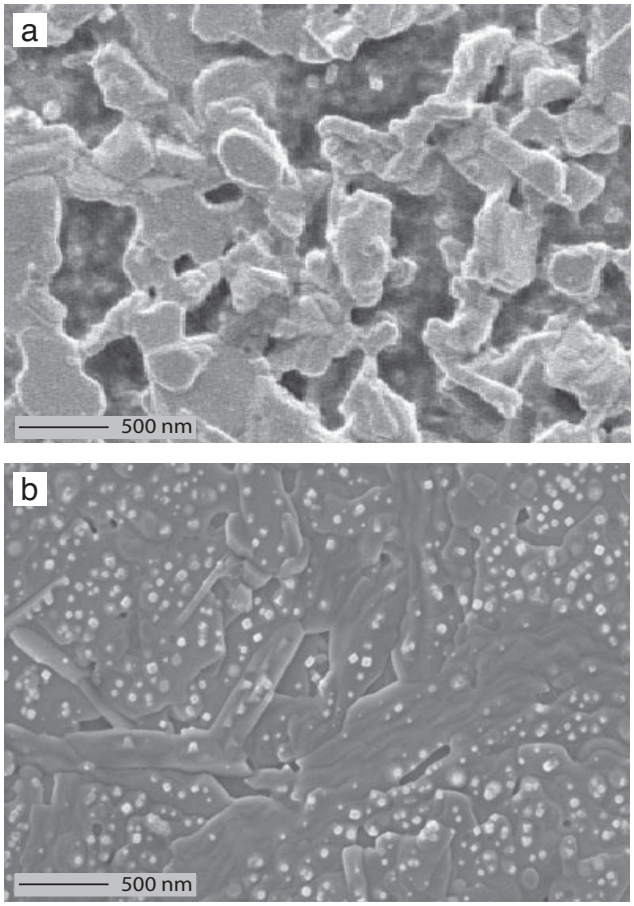


**Fig. 1.** SEM images showing ≈100 nm thick Y123 films on $SrTiO_3$. Films from Batch 1 in (a) show a high porosity. Films from Batch 2 in (b), while laterally more homogeneous, exhibit a granular fine structure, which is probably due to the formation of a second crystalline phase at the film surface.

are aligned with one face parallel to the substrate surface. This indicates a predominantly epitaxial alignment of the Y123 phase with respect to the $SrTiO_3$ substrate. The morphology of films from Batch 2 is different. The visible crystallites in Figure 1b are much larger and the film is laterally more continuous. The crystal faces are less well defined compared to Figure 1a, but the visible terraces indicate epitaxy of the Y123 phase with respect to the substrate also in this case. As opposed to films from Batch 1, Figure 1b shows a granular substructure, which is most likely due to the formation of a crystalline phase at the film surface.

The formation of this crystalline phase at the Y123 film surface seems to be intrinsic to the Batch 2 film preparation procedure. The films deposited from the same precursor solution onto $LaAlO_3$ substrates, shown in Figure 2, are very similar to Figure 1b. The films are laterally continuous, decorated by granules.

None of the samples showed large well defined terraces with vertical crystal planes indicating an in-plane orientation of the superconducting phase. Such a morphology is characteristic for solution deposited Y123 films on

[1] For simplicity, we shall regard the rhombohedral, pseudocubic $LaAlO_3$, $a_{rhomb} = 3.790\,Å$, $c_{rhomb} = 13.11\,Å$ as cubic with an average lattice parameter $a_{cub} = 3.787\,Å$, the average of $a_{rhomb}$ and $c_{rhomb}/(2 \cdot \sqrt{3}) = 3.785\,Å$.

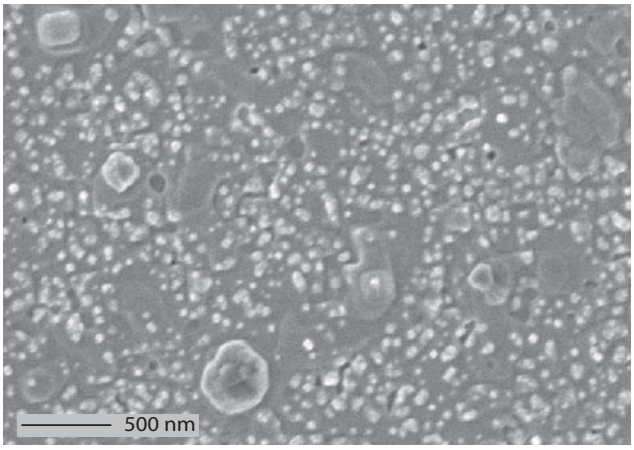


**Fig. 2.** SEM image of a Y123 film on a $LaAlO_3$ substrate, made from the same precursor solution as the the film in Figure 1b. While qualitatively similar, the average crystallite size of both the majority phase and the granular surface structure is reduced compared to Figure 1b.

MgO-(001) substrates [9], Y123 deposited by laser ablation onto $SrTiO_3$-(001) [17], and $Bi_2Sr_2CaCu_2O_x$ films on $SrTiO_3$ that were prepared in a similar way as the Y123 films described here.

### 2.3 Resistance measurements

The resistance of the films was measured in the four point mode. Platinum wires were contacted to the films of Batch 1 by silver paste. The samples were cooled to 50 K in a PPMS 6000 cryostat (Quantum Design, San Diego, USA). The sample resistance $R$ was measured (Agilent multimeter 3458A) as a function of temperature $T$ while heating with a rate of 1 K/min.

The resistance of the Batch 2 samples was measured in a similar way. Gold wires were used to contact the samples. They were cooled in a Cryo-Mini-Refrigerator (Iwatani Corp., Japan). The sample resistance was measured during cooling with 4 K/min. The temperature was controlled by an autotuning temperature controller (Lake Shore Model 330). The current was controlled by a programmable current source (Keithley Model 224) and the voltage measured by a digital voltmeter (Keithley Model 182).

The resistance measurements of Y123 films from Batch 2 on $SrTiO_3$ and $LaAlO_3$ are shown in Figure 3. The films show a clear transition to the superconducting state at 89.6(3) K and 90.0(3) K for the Y123 on $SrTiO_3$ and $LaAlO_3$, respectively. This is comparable to the value of $T_c = 93$ K for Y123 films made by other techniques [1].

The resistance measurements of Batch 1 films showed no superconductive behavior down to 40 K, but instead a monotonous increase in sample resistance with decreasing temperature was observed. This result was repeatedly obtained for several samples on both substrate types. It is therefore likely that the lack of superconducting behavior was characteristic for Batch 1. Since the sample preparation protocols of Batch 1 and 2 were similar, and since the

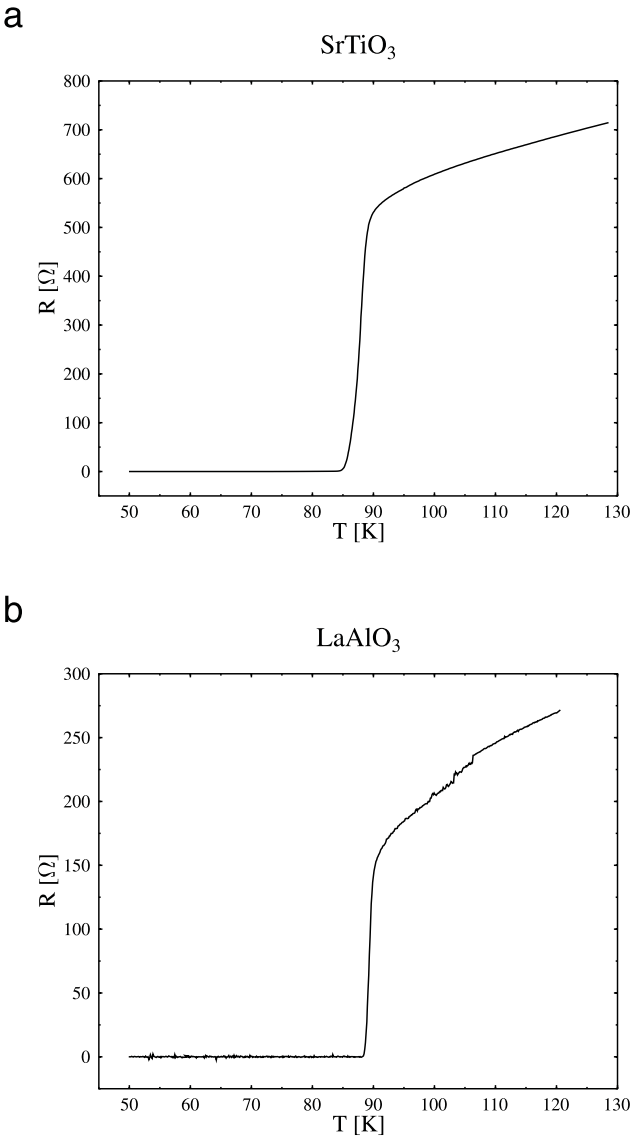


**Fig. 3.** Resistance of Batch 2 films as a function of temperature. (a) The critical temperature for Y123 on $SrTiO_3$ was 89.6(3) K. (b) For Y123 on $LaAlO_3$ $T_c = 90.0(3)$ K.

the protocol of Batch 1 was successfully used to prepare $Bi_2Sr_2CaCu_2O_x$ superconducting thin films on $SrTiO_3$ and $LaAlO_3$ [18], it is instructive to further investigate samples from both batches.

For the superconducting samples (Batch 2), the critical current density was measured after the conclusion of all other experiments. To obtain a well defined lateral sample geometry for transport measurements, 200 $\mu$m wide bridges were etched into the Y123 film, using a photolithographic process. Figure 4 shows the critical current density $J_c$ as a function of temperature. Solution deposited Y123 films on $SrTiO_3$ and $LaAlO_3$ exhibit a low temperature value of $J_c$ of $\sim 10^5$ A/cm$^2$. For Y123 film on $LaAlO_3$ this value of $J_c$ is reached at a relatively high temperature ($\approx$80 K). This compares favorably with

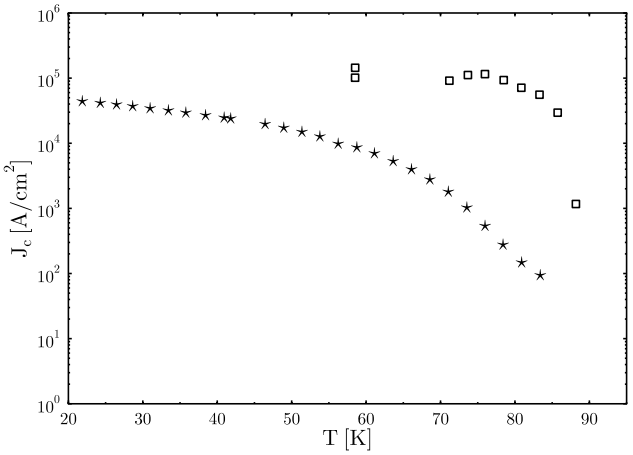


**Fig. 4.** Critical current density $J_c$ of Batch 2 films as a function of temperature for ≈100 nm thick Y123 films on $SrTiO_3$ (⋆) and on $LaAlO_3$ (□) substrates.

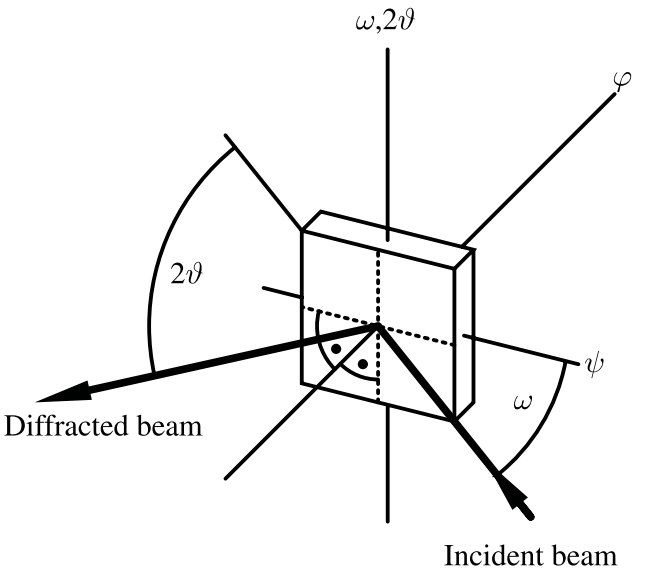


**Fig. 5.** The four axes of a Philips materials diffractometer, shown with $\psi = 0°, \varphi = 0°$.

Y123 films made by other deposition techniques, for which values for $J_c$ of $5 \times 10^5 - 2 \times 10^6$ A/cm$^2$ were reported [1].

### 2.4 X-ray diffraction

The orientation of the Y123 crystallites with respect to the two substrate types was determined using four different X-ray diffraction experiments. To identify the Y123 phase with a **c**-axis orientation parallel to the substrate surface normal (**c**-axis orientation), $\omega$-$2\vartheta$ scans were taken on a Philips X'Pert MRD 3050/65 materials diffractometer (40 kV, 40 mA, X'Pert Data Collector 2.0b software) or on a Philips PW 1820 powder diffractometer (40 kV, 30 mA, APD PW 1877 3.6g software). The quality of the alignment of the **c**-axis oriented Y123 crystals with respect to the substrate was determined by rocking curves ($\omega$ scans) taken on the Philips materials diffractometer. Texture scans ($\varphi - \psi$ scans) revealed the in-plane orientation of the Y123 crystallites (both **c**-axis and **a**-axis oriented) and area scans ($\omega$-$2\vartheta - \psi$ scans) were used to measure the in-plane orientation of the different Y123 domains and to search for additional phases with a highly symmetric lattice plane parallel to the $\mathbf{a} - \mathbf{c}$ plane of $SrTiO_3$ or $LaAlO_3$. Both texture and area scans were performed on the Philips materials diffractometer. All diffractometers were equipped with monochromators for Cu K$\alpha_1$ radiation. The notation of the scan-axes is given in Figure 5.

## 3 Results and discussion

The SEM and resistance measurements show a marked difference between the two sample series (Batch 1 and 2). To improve the reliability of the solution deposition process, it is instructive to investigate the crystallographic properties of samples from both batches on the two substrate types.

Four samples were chosen for further investigation by X-ray diffraction. Figures 6 and 7 show $\omega$-$2\vartheta$ scans taken of samples from Batch 1 and 2 on $SrTiO_3$ and $LaAlO_3$. All four spectra show the $(00l)$ reflections of the substrate material and a set of peaks that can be assigned to the Y123 phase with the **c**-axis oriented parallel to the substrate normal. The differing intensities of the four spectra are due to different scanning conditions in terms of counting time per step.

The quantitative analysis of the $(00l)$ reflections yields the $c$-lattice constant of the **c**-axis oriented Y123 phase. For Y123 from Batch 1, we find values of 11.70(3) Å and 11.63(2) Å for the $SrTiO_3$- and the $LaAlO_3$-substrate, respectively. For samples from Batch 2, we find 11.67(3) Å and 11.67(2) Å, respectively. While the $c$-lattice constants of the Batch 2 samples agree with earlier published values for Y123 films [19–22], the values of Batch 1 samples show a larger variation.

The conductivity (superconductor, semiconductor, or insulator) of $YBa_2Cu_3O_{7-\delta}$ is determined by the oxygen deficiency $\delta$. It is therefore instructive to estimate $\delta$. Since lattice parameters $a$, $b$, and $c$ and the intensity ratios of the X-ray peaks in Figures 6 and 7 are a function of $\delta$, the oxygen deficiency can be obtained by a comparison to published work. Ye and Nakamura [19] measured $a$, $b$, and $c$ and the intensity ratios $I_{(005)}/I_{(006)}$, $I_{(005)}/I_{(004)}$, and $I_{(005)}/I_{(007)}$ as a function of $\delta$ for films on MgO. Cava et al. [20], Ono [21], or Jorgensen et al. [22] give the dependence of $a$, $b$, and $c$ on $\delta$ for bulk samples.

Since $c$ can be easily measured by an $\omega$-$2\vartheta$ scan, this parameter is the first choice for the estimation of $\delta$. But as explained by Ye and Nakamura, lattice defects or cation disorder can influence $c$. Therefore, they also characterized the oxygen content of their samples in terms of the intensity ratios of four measured peaks. For MgO-substrates they find the ratio of the Y123-(006) and (005) peaks best suited to measure $\delta$. Since the Y123-(006) peak coincides

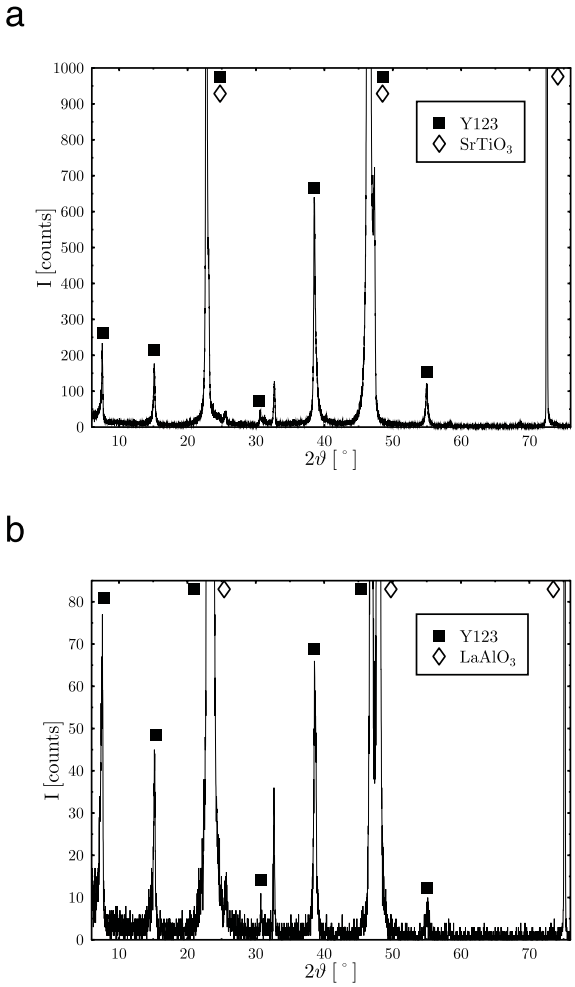


**Fig. 6.** $\omega$-$2\vartheta$ scan of Y123 samples from Batch 1 on $SrTiO_3$ (a) and on $LaAlO_3$ (b). In addition to the substrate and Y123 signal, some further peaks are discernible.

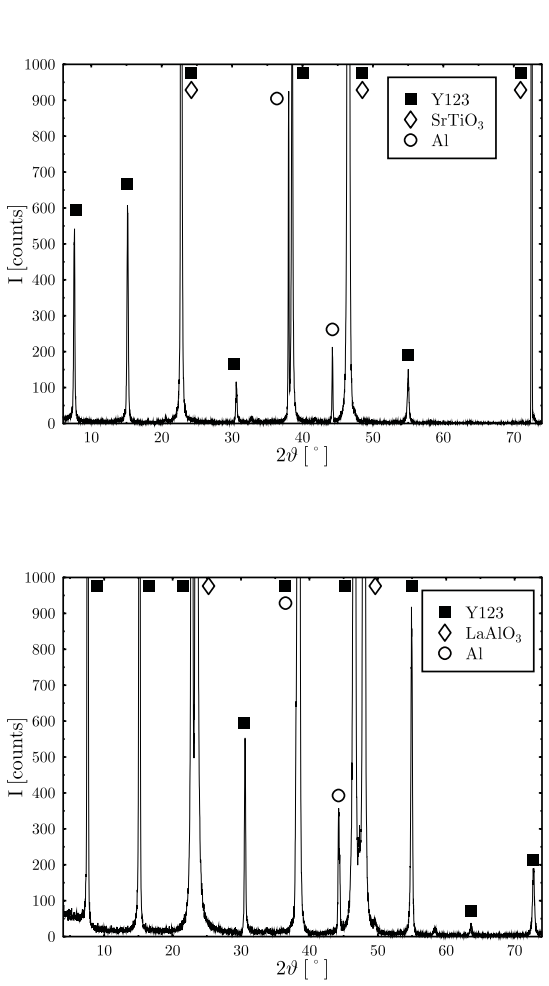


**Fig. 7.** $\omega$-$2\vartheta$ scan of Y123 samples from Batch 2 on $SrTiO_3$ (a) and on $LaAlO_3$ (b). Two of the peaks that arise neither from the Y123 nor from the substrate can be attributed to the (111) and (200) reflections of the aluminum sample support, which was accidentally exposed to the 1 cm wide line focus of the primary beam.

with the (002) peak for $SrTiO_3$ and $LaAlO_3$ substrates, it is more suitable to characterize $\delta$ in terms of the intensity ratios of the Y123 $I_{(005)}/I_{(004)}$ and $I_{(005)}/I_{(007)}$ peaks.

Table 1 gives the values for $\delta$ of our four samples obtained by comparing the measured values of $c$ and the $I_{(005)}/I_{(004)}$ and $I_{(005)}/I_{(007)}$ intensity ratios with the results from references [19–22].

The estimated values of $\delta$ in Table 1 show a large scatter. This may be due to a number of reasons. The epitaxial growth of Y123 on $SrTiO_3$ and $LaAlO_3$ may differ from the Y123 film on MgO considered in [19]. The $c$-lattice constant of our samples may be influenced by other factors than only the oxygen deficiency $\delta$ (e.g. lattice defects, stress). The determination of the peak intensity ratios may be influenced by the overlap with peaks from other phases that are present in the film. Despite the large scatter in the values of $\delta$, the results in Table 1 indicate that all four samples had a high enough degree of oxygenation that is required for the Y123 phase to be superconducting. In particular, the samples from Batch 1 and 2 do not significantly differ in their oxygen content. The difference must therefore lie in the morphology of the Y123 crystallites, rather than the composition of the Y123 phase. Clearly the epitaxial alignment of the Y123 crystallites and their lateral order are of critical importance, in addition to contamination of the Y123 film by other phases.

In Figure 6, peaks that are not attributable to the Y123 phase or the substrate were observed for values of $2\vartheta$ at 25.6°, 32.7°, 47.3°, 58.4°, and 68.6° in Figure 6a and at 25.6° and 32.7° in Figure 6b. Furthermore, also the spectra of Batch 2 samples show additional peaks at 20.6°, 32.7°, and 41.8° in Figure 7a and at 49.6° and 58.3° in Figure 7b. Both in Figures 6 and 7, these peaks have rather low intensities, indicating that the films consist mainly of **c**-axis oriented Y123.

The mosaic spread of **c**-axis oriented Y123 perpendicular to the film plane was further analyzed by $\omega$ scans (so-called rocking curves). Table 2 gives the full width at half maximum (FWHM) of (001) and (002) substrate peaks and the (002) and (005) Y123 peaks for both sample series on both substrate types. The larger mosaic spreads of the

**Table 1.** Oxygen deficiency $\delta$ estimated by comparing the lattice constant $c$ with data from references [19–22] (upper part of the table). In the last two rows of the table, $\delta$ is estimated by comparing the peak intensity ratios $I_{(005)}/I_{(004)}$ and $I_{(005)}/I_{(007)}$, respectively, with reference [19]. $0^*$ denotes calculated values of $\delta$ that are negative or outside the range of values given in the respective publication.

| | Batch 1 | | Batch 2 | |
|---|---|---|---|---|
| | $SrTiO_3$ | $LaAlO_3$ | $SrTiO_3$ | $LaAlO_3$ |
| $c$ [Å] | 11.70(3) | 11.63(2) | 11.67(3) | 11.67(2) |
| $\delta$ [19] | 0–0.15 | $0^*$ | 0 | 0 |
| $\delta$ [20] | 0.15(15) | $0^*$ | $0^*$ | $0^*$ |
| $\delta$ [21] | 0.30(16) | $0^*$(0.03) | 0.14(16) | 0.14(11) |
| $\delta$ [22] | 0.24(20) | $0^*$ | $0^*$ | $0^*$ |
| $I_{(005)}/I_{(004)}$ | 15.25 | 14.50 | 17.07 | 14.80 |
| $I_{(005)}/I_{(007)}$ | 5.08 | 9.67 | 10.86 | 7.02 |
| $\delta$ [19] | 0–0.15 | 0–0.15 | 0.05–0.20 | 0–0.15 |
| $\delta$ [19] | 0.15–0.25 | $0^*$ | $0^*$ | $0^*$ |

**Table 2.** Peak width (full width at half maximum) of the rocking curves ($\omega$ scans) of selected peaks. The Y123 (005) reflection of the Batch 2 sample on $LaAlO_3$ could not be measured due to an overlap with the spurious signal stemming from the Al sample holder (see Fig. 7).

| Batch | Substr. | Substrate | | Y123 | |
|---|---|---|---|---|---|
| | Peak | (001) | (002) | (002) | (005) |
| 1 | $SrTiO_3$ | 0.03° | 0.03° | 0.58° | 0.53° |
| 1 | $LaAlO_3$ | 0.04° | 0.04° | 0.74° | 0.74° |
| 2 | $SrTiO_3$ | 0.05° | 0.05° | 0.32° | 0.37° |
| 2 | $LaAlO_3$ | 0.05° | 0.05° | 0.25° | – |

samples made from Batch 1 precursors indicate a somewhat lower quality of the epitaxial order of the Y123 films. The angular spreads of the Batch 2 samples are, on the other hand, comparable to values found for PLD grown films [23,24].

To establish the in-plane orientation of the Y123 crystals, textures scans ($\varphi - \psi$ scans) were performed. The substrates were aligned on a four-axis diffractometer using the substrates' (101) and (002) reflections so that at $\varphi = 0°$ the substrate-[100] direction was in the plane of diffraction. Since the Y123-{104} reflections do not overlap with any of the substrate peaks they were chosen to investigate the orientation of the $\mathbf{a}_{Y123}$- and $\mathbf{b}_{Y123}$-axes, with lattice constants of $a = 3.82$ Å, $b = 3.89$ Å [20,22]. The Y123-{104} texture scan of a Batch 2 sample on $SrTiO_3$ is shown in Figure 8. With $c \approx 3.1 \cdot a$, the (104) direction forms an angle of approx. 37.8° with the **c**-axis. Therefore, for **c**-axis oriented material the {104} reflections appear at $\psi = 37.8°$. Assuming a 'cube on cube'-type growth of Y123, where the **a**-axis of Y123 is parallel to the **a** or **b** substrate directions, the Y123-{104} reflections should appear at $\varphi = 0°, 90°, 180°, 270°$. This is borne out

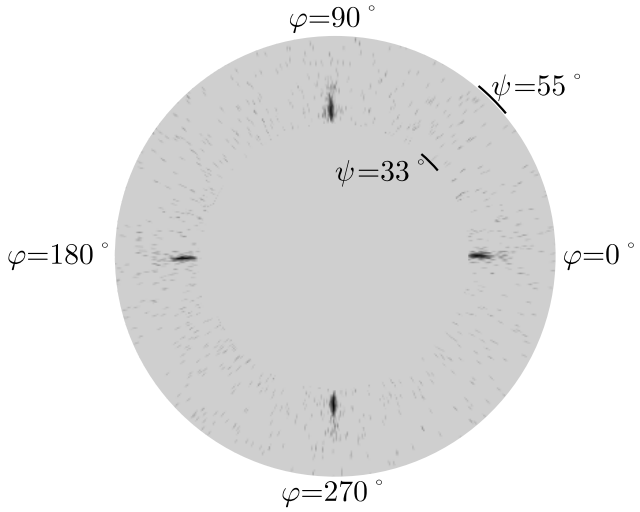


**Fig. 8.** Texture scan ($\varphi - \psi$ scan) of the Y123-{104} reflections of a Batch 2 sample on $SrTiO_3$. The elongated peak shape is a consequence of the X-ray beam profile ($1 \times 10\,mm^2$ line focus).

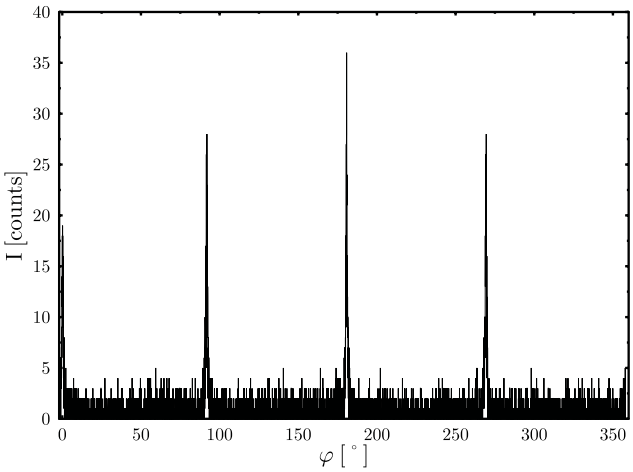


**Fig. 9.** $\varphi$ scan of the sample from Figure 8 for $\psi = 37.39°$. The averaged width of the four peaks is 0.36(15)°.

by the data in Figure 8, showing four strong peaks at the predicted positions. In Figure 9, a single $\varphi$ scan taken for $\psi = 37.39°$ shows the peak positions in more detail. The four peaks are centered at $\varphi = 0.2°, 91.9°, 180.7°, 269.5°$ and have an average FWHM of 0.36(15)°. The angular spread is smaller than that found for Y123 films on $LaAlO_3$ by CVD [6] of ≈1.5°.

In Figure 8 only peaks stemming from the **c**-axis oriented Y123 phase are visible. No traces of Y123 domains with other orientations are discernible. In particular, no **a**-axis oriented Y123 is seen, which is known to grow preferably at lower temperatures [25–27]. For the Y123-{104} texture scan of the Batch 1 sample in Figure 10 four additional peaks are discernible at higher values of $\psi$. The peaks at $\psi = 52.2°$ and $\varphi = 0°, 90°, 180°, 270°$ can be attributed to **a**-axis oriented Y123 [3,26,28]. Neither of the texture scans shows indications for **c**-axis oriented material with an alignment of the **a**-axis parallel to the [110] substrate

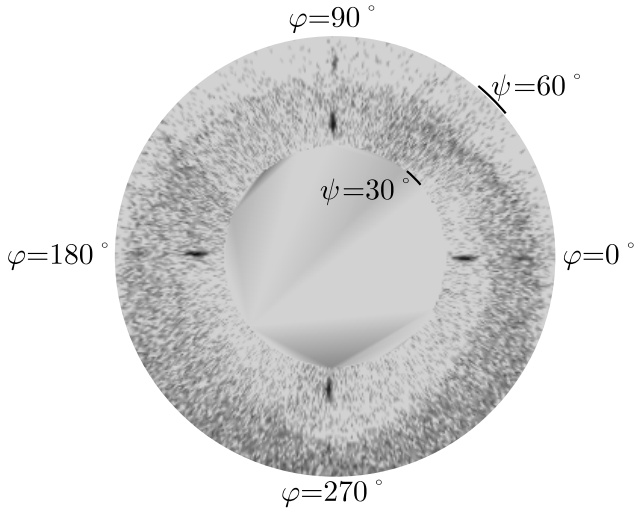


**Fig. 10.** Texture scan ($\varphi - \psi$ scan) of the Y123-{104} reflections of a Batch 1 sample on $LaAlO_3$. The four stronger peaks of the **c**-axis oriented Y123 (inner ring) and the four weaker peaks of the **a**-axis oriented Y123 (outer ring) are clearly discernible.

direction, as was reported for Y123 on MgO, grown at lower temperatures [27].

The appearance of some (but not all) of the additional peaks in the $\omega$-$2\vartheta$ scans (Figs. 6 and 7) for both Batch 1 and 2 samples can be explained by the assumption that a small amount of the Y123 phase has a random orientation. For example the peaks at $2\vartheta = 32.7°$ could be the sum of (013), (103), and (110) reflections, all of which belong to the strongest reflections of Y123. A non-epitaxial Y123 phase gives rise to rings in the area scans, fragments of which can be seen in Figure 12 for the strongest Y123 reflections. Note that the additional peaks in the $\omega$-$2\vartheta$ scans are much weaker for the Batch 2 samples than for the Batch 1 samples.

Judging by these results, differences between Batch 1 and 2 samples are (1) the amount of non-epitaxial (non **c**-axis oriented) Y123 material and (2) the quality of the alignment of **c**-axis oriented Y123. These morphological differences seem to be responsible for the difference in conductivity. The sensitivity to minor changes in the preparation of Y123 films is in contrast to the rather robust solution deposition of $Bi_2Sr_2CaCu_2O_x$ using a similar procedure.

Figures 11 and 12 show the area scans of the Batch 2 sample on $SrTiO_3$ and the Batch 1 sample on $LaAlO_3$, respectively. Both figures show two columns of peaks that can be attributed the substrate and **c**-axis oriented Y123. In Figure 12, the $LaAlO_3$-(101) peak is surrounded by four Y123 peaks. The upper and lower peak belong to the **c**-axis oriented Y123, while the left and right peak belong to **a**-axis oriented material.

The reciprocal $\mathbf{a}^*\mathbf{c}^*$ lattice plane was chosen because it contains the ($h0l$) reflections of the substrates and the ($h0l$) reflections of **c**-axis oriented Y123 with an in-plane orientation where $\mathbf{a}_{Y123}$ lies parallel to $\mathbf{a}_{substrate}$. The appearance of the peaks in Figures 11 and 12 confirms the

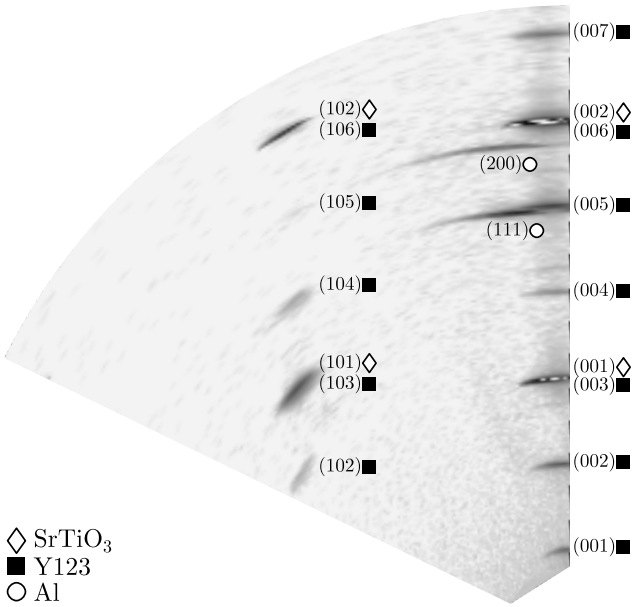


**Fig. 11.** Area scan of the $\mathbf{a}^*\mathbf{c}^*$ plane of a Batch 2 sample on $SrTiO_3$. The peaks are indicative of **c**-axis aligned Y123 with an **a**-axis alignment parallel to the **a**-axis of $SrTiO_3$. The two smeared-out Al lines stem from the sample holder.

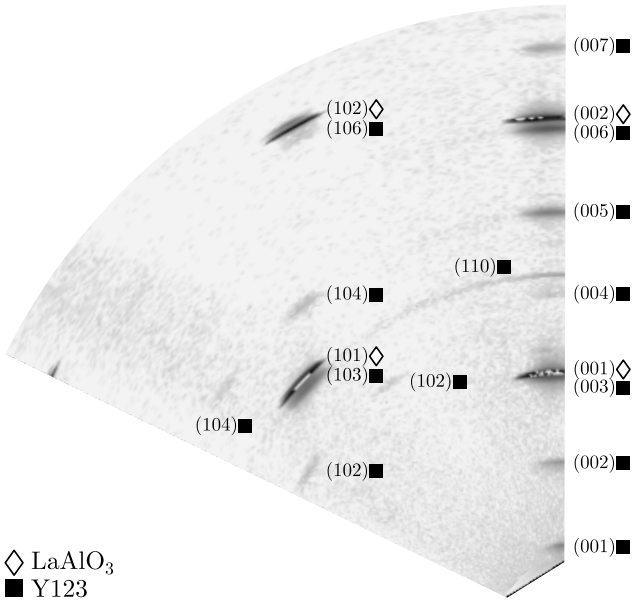


**Fig. 12.** Area scan of the $\mathbf{a}^*\mathbf{c}^*$ plane of a Batch 1 sample on $LaAlO_3$. Two peaks reveal the presence of **a**-axis oriented Y123.

results of the texture scans (Figs. 8 and 10) and the absence of other peaks is a strong indication that only the Y123 phase has grown epitaxially.

## 4 Conclusion

In summary, we have investigated the epitaxial order of Y123 films that were solution deposited onto $SrTiO_3$ and

$LaAlO_3$ substrates. The films consisted mainly of Y123, the majority of which had grown with the **c**-axis perpendicular to the substrate surface and with the **a**-axis oriented parallel to the **a**- and **b**-axis of the substrate.

Similarly prepared samples were found to be either superconducting with a critical temperature of $\approx$90 K and a critical current density of $\sim 10^5$ A/cm$^2$, or semiconducting down to low temperatures. Since the lattice parameters of both sample types were very similar, it is unlikely that this difference arises from a different chemical composition (oxygenation) of the Y123 phase.

Whether a Y123 film is superconducting or not can be correlated to the SEM images and the X-ray diffraction results described in this study. The main differences between the two sample batches were:

1. The film morphology. Superconducting Y123 films were laterally homogeneous, while non-superconducting films were highly porous.
2. The amount of contaminant phases, which can be identified by the stronger additional peaks in the $\omega$-$2\vartheta$ scans.
3. The appearance of a granular structure on top of an otherwise continuous surface for Batch 2 samples. While this surface phase requires further examination, it is possible that it stems from a non-superconducting phase (additional peaks in Fig. 7). Such a location of a redundant minority phase would affect the electronic properties of the underlying film only little.

Since Batch 1 samples consist mainly of the **c**-axis oriented Y123 phase, we postulate that the lack of a transition to a superconducting state arises from a combination of the effects listed above. Both, the high porosity and the presence of an unidentified (presumably non-superconducting) phase potentially reduces the lateral connectivity of the Y123 **c**-axis oriented epitaxial phase. A complete loss of the lateral connectivity of the Y123 phase would lead to an electrical conductivity that is determined by the material with lowest conductivity. The differences in porosity and contaminant phases of Batch 1 and 2 samples arise possibly from the somewhat different annealing protocols.

Despite its apparent sensitivity to details in the film preparation, the manufacture of Y123 by a liquid deposition process is useful. The experimental procedure we have used is much more simple and less expensive compared to more established deposition methods. In addition, layers made by solution deposition processes can easily be patterned by soft-lithography [12] to manufacture superconducting thin films with lateral structures on the submicrometer scale [29].

The authors thank U. Wiesner, R. Ullrich, and S. Walheim for their important role in the initial phase of this project, T.T.M. Palstra for access to his cryostat and J. Baas for his help with the resistance measurements. The SEM images were taken by H. Nijland and some of the PMAA was synthesized by W. Belgraver. Partial financial support was provided by the Dutch "Stichting voor Fundamenteel Onderzoek der Materie" (FOM).

## References

1. *European White Book on Materials Science*, `www.mpg.de/bilderBerichteDokumente/dokumentation/europWhiteBook/`
2. C. Maréchal, E. Lacaze, W. Seiler, J. Perrière, Phys. C **294**, 23 (1998)
3. R. Kromann, J.B. Bilde-Sørensen, R. de Reus, N.H. Andersen, P. Vase, T. Freltoft, J. Appl. Phys. **71** (7), 3419 (1992)
4. D. Dimos, P. Chaudhari, J. Mannhart, Phys. Rev. B **41** (7), 4038 (1990)
5. J. Stejskal, J. Leitner, D. Sedmidubský, M. Nevřiva, P. Beran, A. Strejc, J. Cryst. Growth **210**, 587 (2000)
6. A. Ignatiev, P.C. Chou, Y. Chen, X. Zhang, Z. Tang, Phys. C **341-348**, 2309 (2000)
7. R. Krupke, Z. Barkay, G. Deutscher, Physica C **317-318**, 536 (1999)
8. L.F. Admaiai, P. Grange, B. Delmon, M. Cassart, J.P. Issi, J. Mat. Sci. **29**, 5817 (1994)
9. S.R. Breeze, S. Wang, J. Mat. Sci. **34**, 1099 (1999)
10. C.E. Rice, R.B. van Dover, G.J. Fisanick, Appl. Phys. Lett. **51** (22), 1842 (1987)
11. I. von Lampe, F. Zygalsky, G. Hinrichsen, H. Springer, H. Schubert, J. Mat. Sci. Lett. **21**, 133 (2002)
12. Y. Xia, J.A. Rogers, K.E. Paul, G.M. Whitesides, Chem. Rev. **99** (7), 1823 (1999)
13. E. Schäffer, T. Thurn-Albrecht, T.P. Russell, U. Steiner, Nature **403**, 874 (2000)
14. E. Schäffer, S. Harkema, M. Roerdink, R. Blossey, U. Steiner, Adv. Materials **15** (6), 514 (2003)
15. I. von Lampe, S. Götze, F. Zygalsky, J. Low Temp. Phys. **105** (5, 6), 1289 (1996)
16. J.C.W. Chien, B.M. Gong, J.M. Madsen, R.B. Hallock, Phys. Rev. B **38**, 11853 (1988)
17. X. Zhu, G.C. Xiong, R. Liu, Y.J. Li, G.J. Lian, Z.Z. Gan, Phys. C **216**, 153 (1993)
18. O.F. Göbel, X. Du, T. Hibma, I. von Lampe, U. Steiner, Eur. Phys. J. B **39**, 149 (2004)
19. J. Ye, K. Nakamura, Phys. Rev. B **48** (10), 7554 (1993)
20. R.J. Cava, B. Batlogg, C.H. Chen, E.A. Rietman, S.M. Zahurak, D. Werder, Phys. Rev. B **36** (10), 5719 (1987)
21. A. Ono, Jpn J. Appl. Phys. **26**, L1223 (1987)
22. J.D. Jorgensen, B.W. Veal, A.P. Paulikas, L.J. Nowicki, G.W. Crabtree, H. Claus, W.K. Kwok, Phys. Rev. B **41** (4), 1863 (1990)
23. D. Berling, A. Del Vecchio, G. Leggieri, B. Loegel, A. Luches, A. Mehdaoui, L. Tapfer, Sol. State Comm. **97** (8), 657 (1996)
24. M. Rajeswari, R. Shreekala, Z. Trajanovic, S.B. Ogale, D.D. Chougule, T. Vankatesan, S. Lakeou, A.N. Thorpe, Phys. C **304**, 277 (1998)
25. E. Sodtke, C. Andrzejak, D. Guggi, Y. Xu, Phys. C **180**, 50 (1991)
26. F. Sandiumenge, J. Santiso, A. Figueras, J. Appl. Phys. **76** (5), 2951 (1994)
27. B.C. Chung, C.H. Tsai, S.S. Hsu, C.C. Yu, C.H. Lin, I.N. Lin, Phys. C **227**, 357 (1994)
28. M. Mukaida, S. Miyazawa, Jpn J. Appl. Phys. **32**, 4521 (1993)
29. O.F. Göbel, U. Steiner, in preparation